

Time lag between metamorphism and crystallization of anatetic granites (Córdoba, Argentina)

F.J. D'Eramo^{1,2} J.J. Esteban^{3*} M. Demartis^{1,2} E. Aragón⁴ J.E. Coniglio^{1,2} L.P. Pinotti^{1,2}

¹Instituto de Ciencias de la Tierra, Biodiversidad y Ambiente (ICBIA) CONICET-UNRC

Ruta Nac. nº 36 km 601, Río Cuarto, Argentina

²Universidad Nacional de Río Cuarto, Departamento de Geología

Ruta Nac. nº 36 km 601, Río Cuarto, Argentina. D'Eramo e-mail: deramo@exa.unrc.edu.ar; Demartis e-mail: mdemartis@exa.unrc.edu.ar; Pinotti e-mail: lpinotti@exa.unrc.edu.ar; Coniglio e-mail: jconiglio@exa.unrc.edu.ar

³Departamento de Geología, Facultad de Ciencia y Tecnología,
Universidad del País Vasco UPV/EHU

Apartado 644, 48080 Bilbao, Spain. Esteban e-mail: jj.esteban@ehu.es

⁴Universidad Nacional de la Plata, CIG-CONICET

Diagonal 113 64, 1900. La Plata, Argentina. Aragón e-mail: aragoneugenio2020@gmail.com

*Corresponding author

ABSTRACT

SHRIMP and LA-ICP-MS analyses carried out on zircons from the Río de los Sauces granite revealed their metamorphic and igneous nature. The metamorphic zircons yielded an age of 537 ± 4.8 (2 σ) Ma that probably predates the onset of the anatexis during the Pampean orogeny. By contrast, the igneous zircons yielded a younger age of 529 ± 6 (2 σ) Ma and reflected its crystallization age. These data point to a short time lag of *ca.* 8 Myr between the High Temperature (HT) metamorphic peak and the subsequent crystallization age of the granite. Concordia age of 534 ± 3.8 (2 σ) Ma, for both types of zircon populations, can be considered as the mean age of the Pampean HT metamorphism in the Sierras de Córdoba.

KEYWORDS | Pampean Orogeny. Pampean Metamorphism. Río de los Sauces granite. U-Pb SHRIMP dating. LA-ICP-MS analyses.

INTRODUCTION

The Neoproterozoic to middle Cambrian Pampean orogen ([Aceñalaza and Toselli, 2009](#)), located at the north-central part of Argentina ([Fig. 1](#)), was part of the Terra Australis orogen at the western margin of Gondwana ([Cawood, 2005](#)). It was defined as a paired belt, with calc-alkaline magmatic rocks in the eastern belt and medium- to high-grade metamorphic rocks with peraluminous granites in the western belt ([Rapela et al., 1998](#); [Schwartz et al.,](#)

[2008](#)). This calc-alkaline magmatism is widely exposed in the Sierra Norte de Córdoba and is usually referred to as the Sierra Norte-Ambargasta batholith ([Iannizzotto et al., 2013](#); [Lira et al., 1997](#); [Schwartz et al., 2008](#); [Von Gosen and Prozzi, 2010](#)). The U-Th-Pb dating in granitoids from the Sierra Norte-Ambargasta batholith gave crystallization ages between 530 and 537 Ma and were linked to the development of a continental magmatic arc in an eastward subduction of oceanic lithosphere down to the western

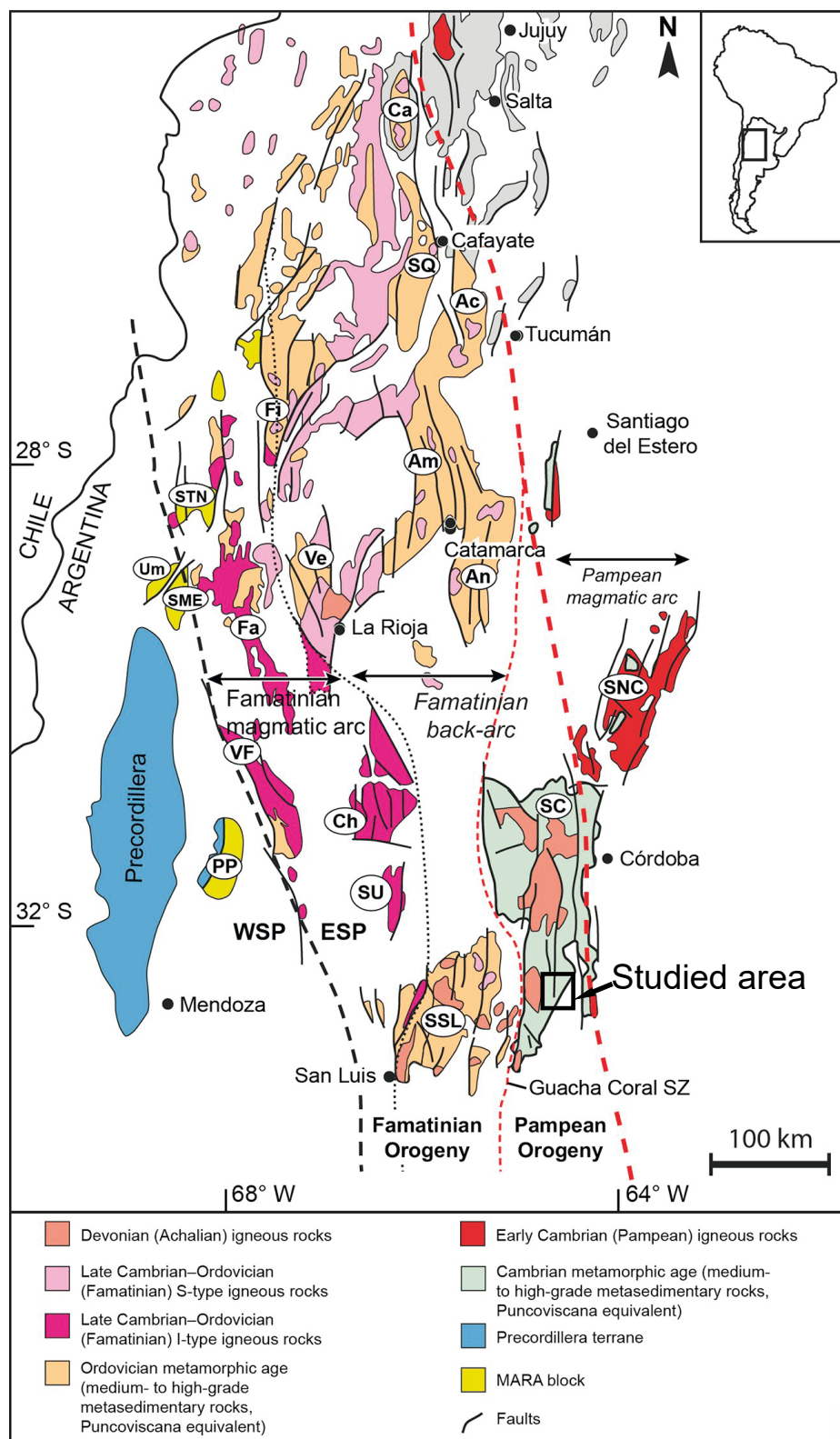


FIGURE 1. Schematic geological map of NW Argentina showing the Sierras Pampeanas geological province, the main mountain ranges, the geological subdivisions, and the extent of the Pampean orogeny (from Weinberg et al., 2018). The location of Figure 2 is shown. Mountain ranges: Sierra de Aconquija (Ac), Sierra de Fiambala (Fi), Sierra de Ambato (Am), Sierra de Ancasti (An), Sierra de Cachi (Ca), Sierra de Velasco (Ve), Sierra de Famatina (Fa), Sierra de Maz-Espinal (SME), Sierra de Valle Fértil (VF), Sierra de Chepes (Ch), Sierra de Ulapes (SU), Sierra de Pie de Palo (PP), Sierras de Córdoba (SC), Sierra de Quilmes (SQ), Sierra Norte de Córdoba (SNC), Sierra de San Luis (SSL), Sierra de Toro Negro (STN), Sierra de Umango (Um), Western Sierras Pampeanas (WSP), Eastern Sierras Pampeanas (ESP).

margin of Gondwana (Casquet *et al.*, 2018; Dahlquist *et al.*, 2016; Iannizzotto *et al.*, 2013; Rapela *et al.*, 1998; Schwartz and Gromet, 2004; Schwartz *et al.*, 2008; Weinberg *et al.*, 2018).

The western belt of the Pampean orogen is formed mainly of sedimentary and metasedimentary rocks deposited during Neoproterozoic times. These sequences are represented by the low-grade metamorphosed turbidites of the Puncoviscana Formation, and their higher metamorphic grade counterparts (schists, gneisses and migmatites) located at the Sierras de Ancasti and Córdoba (Aceñolaza and Aceñolaza, 2007; Omarini, 1999; Rapela *et al.*, 1998; Rapela *et al.*, 2007; Schwartz and Gromet, 2004; Toselli, 1990; Turner, 1960). There is a lack of consensus regarding the tectonic setting of deposition of the Puncoviscana Basin (Casquet *et al.*, 2018). This has been interpreted as either a 1,000 km long passive margin along the western margin of Gondwana (Ježek *et al.*, 1985; Schwartz and Gromet, 2004) or a fore-arc basin (Hauser *et al.*, 2011; Rapela *et al.*, 2007). The onset of subduction turned these sequences into an accretionary prism leading to medium to high-grade schists, gneisses, and migmatites (Weinberg *et al.*, 2018 and references therein).

The Sierras de Córdoba are located at the southernmost part of the Eastern Sierras Pampeanas, central Argentina (Fig. 1). They are constituted by N-S trending mountain ranges mostly composed of Neoproterozoic to Devonian metasedimentary and igneous rocks. The main tectono-thermal event registered in the Sierras de Córdoba, during the Pampean orogeny, is the so called M₂ (Casquet *et al.*, 2018; Guereschi and Martino, 2014; Rapela *et al.*, 1998). This event was linked to an increase in the P-T conditions, due to crustal shortening with thrusts propagating into the fore-arc (Weinberg *et al.*, 2018), leading to an upper amphibolite to granulite facies metamorphism and anatexis. The anatexis transformed the protoliths (gneisses and schists) into metatexies and diatexites, with associated peraluminous magmatism. The M₂ event reached temperatures above 800°C at mid-crustal pressures of 8–9 kb (Fagiano, 2007; Otamendi *et al.*, 2004; Rapela *et al.*, 1998; Weinberg *et al.*, 2018). This crustal thickening was followed by adiabatic decompression leading to massive crystallization of cordierite in rocks that experienced subsequent partial melting after the first onset of anatexis (Casquet *et al.*, 2018; Otamendi *et al.*, 2004; Weinberg *et al.*, 2018). The timing of these metamorphic events (crustal thickening and adiabatic decompression) has been bracketed between 550 and 515 Ma, according to U-Pb SHRIMP dating in zircons and monazites from different gneisses and migmatites of the Sierras de Córdoba (Rapela *et al.*, 1998; Siegesmund *et al.*, 2010; Sims *et al.*, 1998; Weinberg *et al.*, 2018), thus concluding that the Pampean orogeny lasted for at least 35 Myr.

Geological and geochronological studies dealing with regional metamorphism (M₂) and peraluminous granites derived from the anatetic events of the Pampean orogeny, in the Sierras de Córdoba, are concentrated in the north, mainly in El Pilón complex (Rapela *et al.*, 1998; Rapela *et al.*, 2002; Stuart-Smith *et al.*, 1999). The HT metamorphism and the probably coeval magmatism, were dated in 522 Ma (Rapela *et al.*, 1998). Studies on other Pampean peraluminous granitoids generated during high-grade metamorphism in other parts of the Sierras de Córdoba, are scarce (Escayola *et al.*, 2007; Tibaldi *et al.*, 2008). The lack of geochronological data limits our knowledge on the age of the metamorphic climax, the anatexis, and their temporal relationships with the syntectonic granites of the studied region.

The temporal relationship between metamorphism and granite crystallization differ from orogen to orogen (Esteban *et al.*, 2015; Keay *et al.*, 2001; Vanderhaeghe *et al.*, 1999; Whitney *et al.*, 2003). Although the age of each of these processes can be obtained separately from migmatites and anatetic granites, Esteban *et al.* (2015) demonstrated that zircons extracted from one pluton may be enough to detect the time lag between the metamorphic peak and the magmatic activity in internal domains of orogenic belts. They found a time span of 7 Myr between the metamorphic climax and the emplacement of the Lys-Caillaous pluton in the Axial Zone of the Pyrenees (southern France), by recognizing two populations of zircons, one with igneous and the other one with metamorphic affinities.

Here, we report a rather similar case in the Río de los Sauces granite, Sierra de Comechingones (Argentina), where two distinct zircon populations identified by LA-ICP-MS geochemistry and dated by U-Th-Pb SHRIMP analyses, allowed us to establish the time lag between the metamorphic climax and the crystallization of the granite.

FIELD RELATIONSHIPS AND PETROGRAPHY OF THE RÍO DE LOS SAUCES GRANITE

In this work, we defined a new granitic body, the Río de los Sauces granite, located two kilometers to the north of Río de los Sauces village (Fig. 2A, B). The country rocks are garnet-rich gneisses and metatexite migmatites of the Calamuchita Metamorphic complex (Otamendi *et al.*, 2004). These rocks show an ENE–WSW-trending foliation (S₂) with high angle dips (generally >70°) both to the south and the north. This foliation is parallel to the axial plane of the tight, isoclinal folds and is associated with constrictional non-coaxial strain (Martino and Guereschi, 2014 and references therein). The mineral assemblage of the gneisses is biotite+plagioclase+quartz+garnet, whereas the metatexies are mainly stromatites

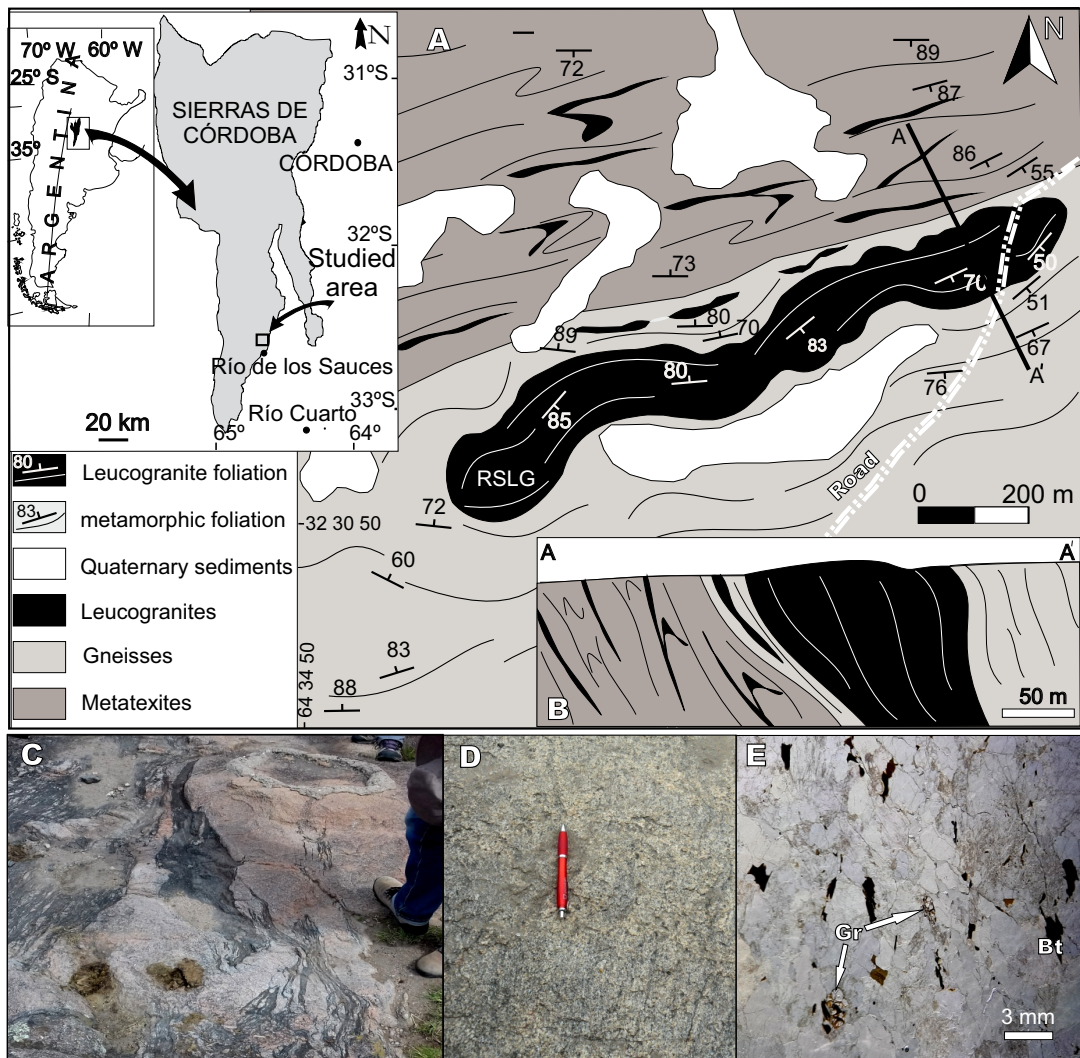


FIGURE 2. A) Geological map of the sheet-shaped Río de los Sauces Leucogranite (RSLG). Inset shows its location in the Sierras de Córdoba, central Argentina. B) Cross-section along profile A-A'. C) Field picture showing relationships between leucosomes and pluton. D) RSLG on outcrop and E) on microphotograph, showing the foliation defined by oriented biotite. Gr: garnet; Bt: biotite.

that contain leucosomes composed of quartz+plagioclase+K-feldspar±biotite±garnet and melanosomes composed of biotite+garnet+quartz+plagioclase+sillimanite.

There are a few examples of leucosomes of stromatites that form phacoliths or patches within boudin necks, evidencing that melting took place during folding. Folded, layer-parallel leucosomes also merge continuously with leucosomes parallel to axial-plane foliation. [Otamendi et al. \(2004\)](#) described similar structures and interpreted them in the same way. Magma transfer through this fold-assisted leucosomes network has been described in other parts of the world ([Weinberg and Mark, 2008](#)). Finally, leucosomes coalesced giving rise to leucogranite and pegmatite sheets, and small plutons. Because of the continuous link from leucosomes to larger sheets and plutons ([Fig. 2C](#)), we interpret that leucogranites are autochthonous granites.

The Río de los Sauces granite was formed by the coalescence of numerous leucogranite sheets, which intruded concordantly the gneisses, close to the gneiss-metataxite boundary ([Fig. 2A, B](#)). The resulting granite body is 1.2 km long and 100–150 m wide. The regional metamorphic foliation trend deflects around the Río de los Sauces granite, implying that after solidification, it also behaved as a competent body during continued deformation. This is a hypidiomorphic coarse-grained leucogranite with a mineral association of microcline+quartz+plagioclase+biotite+muscovite+garnet±sillimanite, and accessories such as zircon, titanite and apatite. The modal proportion of main minerals is: microcline (35–50%) quartz (35–45%) and plagioclase (20–30%). It also shows late patches and pegmatite sheets. The Río de los Sauces granite is weakly foliated. The foliation is defined by oriented biotite and elongated quartz ([Fig. 2D, E](#)), and is parallel to the contacts and the gneiss structures.

U-Th-Pb SHRIMP GEOCHRONOLOGY

One sample from the Río de los Sauces granite ($32^{\circ}30'37.7''\text{S}/64^{\circ}34'18.8''\text{W}$) was processed according to routine zircon mineral separation (crushing, grinding, sieving under $250\ \mu\text{m}$, Wilfley table and methylene iodide) at the University of Río Cuarto (Argentina), in order to date the emplacement of the pluton. The selected zircons were mounted in epoxy resin together with the TEMORA 2 reference zircon (416.78Ma; Black *et al.*, 2004), sectioned, polished and analyzed on a SHRIMP-IIe/MC at the Centro de Pesquisas Geocronológicas of the University of São Paulo (GeoLab-IGe-USP; Brazil). The obtained U-Pb ion microprobe data were processed with the SQUID and Isoplot/Ex 3.00 (Ludwig, 2003) software programs and are presented in Table 1. In order to select target areas, cathodoluminescence (CL) images were obtained by a FEI Quanta 250 Scanning Electron Microscope and XMAX CL detector, in the same laboratory. Further details on the sample preparation, analytical setup, acquisition and data processing are given in Sato *et al.* (2014).

According to CL images (Fig. 3) the zircons reveal a complex zoned pattern characterized by dark luminescent rims developed mainly over xenomorphic cores, and dark luminescent idiomorphic zircons with weak oscillatory zoning and extremely low Th/U ratios (<0.02) (Table 1: spots 9.1; 3.1; 4.1; 16.1; 11.1; 6.1; 8.1; 1.1; 2.1). These zircons contrast with those zircons showing euhedral morphology (prismatic or bipyramidal), concentric undisturbed oscillatory growth zoning, sometimes with progressively U-rich low luminescent rims, lack of inherited xenomorphic cores and high Th/U ratios (0.22–

0.57) (Table 1: spots 1.2; 2.2; 5.1; 12.1; 7.1; 15.1; 14.1; 13.1; 10.1). All these different features point to two discrete zircon populations, ZP₁ and ZP₂.

Nine and eight spot analyses were carried out (Table 1) yielding $^{206}\text{Pb}/^{238}\text{U}$ Concordia ages of 537 ± 4.8 (2σ) (Fig. 4A) and 529 ± 6 (2σ) Ma (Fig. 4B) for ZP₁ and ZP₂, respectively. Although the Concordia age of ZP₂ displays a high Mean Squared Weighted Deviation (MSWD) and low probability of concordance (Fig. 4B), the less discordance analyses (<10 %) yield a weighted mean age of 530 ± 8 (2σ) Ma. A high probability of age coherence in both zircon populations is indicated by the overlapping of the concordant data as they define a Concordia $^{206}\text{Pb}/^{238}\text{U}$ age of 534 ± 3.8 (2σ) Ma (Fig. 4C).

TRACE AND RARE EARTH ELEMENT ANALYSES BY LA-ICP-MS

Trace and Rare Earth Elements (REE) on both zircon populations were analyzed by LA-Q-ICP-MS (Laser Ablation Quadrupole Inductively Coupled Plasma Mass Spectrometry) at the University of the Basque Country (SGIker) using a 213nm New Wave Nd:YAG laser, with a $\sim 3.65\text{J/cm}^2$ energy density at a repetition rate of 10Hz, coupled to a Thermo iCAP Qc quadrupole ICP-MS. The analytical spot size was $40\mu\text{m}$ in diameter, and in most cases, the zircons were completely pierced through during the 60 seconds of acquisition time. External calibration was performed to the NIST SRM 612 (Jochum *et al.*, 2011). The internal standard was the stoichiometry-calculated ^{90}Zr , and data reduction was carried out by the

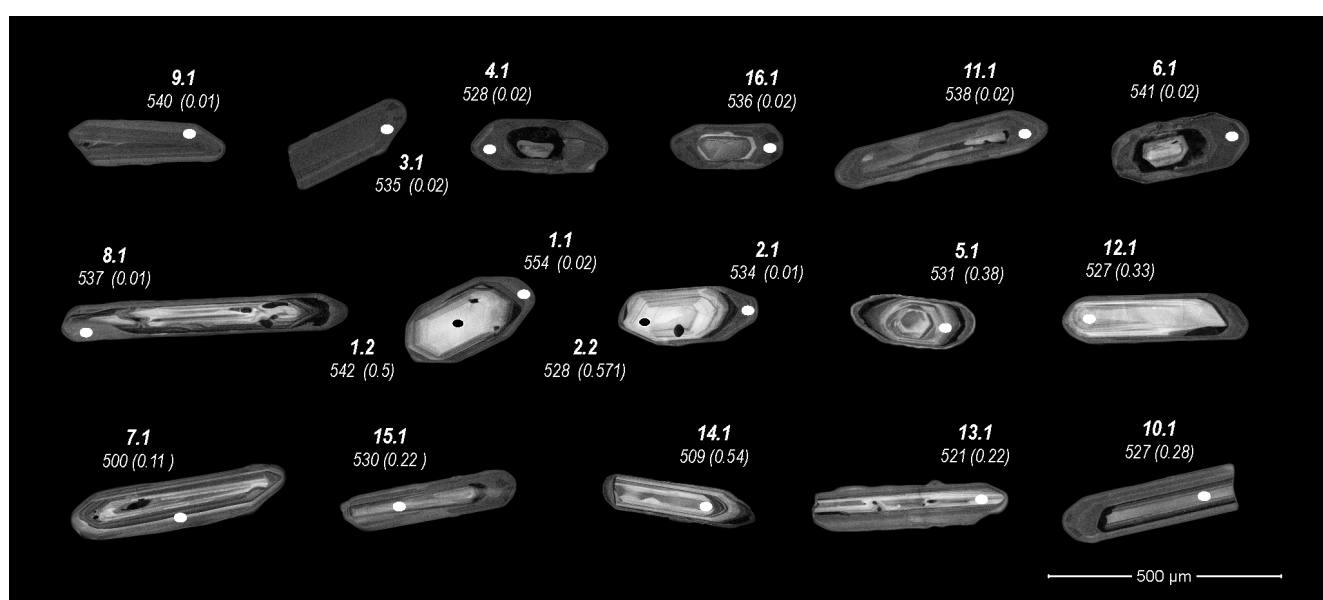


FIGURE 3. Cathodoluminescence images of the analyzed zircons from the Río de los Sauces granite. Labels indicate spot numbers (in bold), corresponding $^{206}\text{Pb}/^{238}\text{U}$ ages and Th/U ratios (in parentheses).

TABLE 1. SHRIMP U-Pb isotopic data for analyzed zircon populations from the Río de Los Sauces Granite. Data are arranged according to Th/U value

Spot	$^{206}\text{Pb}_c$ (%)	U (ppm)	Th (ppm)	Th/U	* $\frac{^{206}\text{Pb}}{^{238}\text{U}}$ Age (Ma)	* $\frac{^{207}\text{Pb}}{^{206}\text{Pb}}$ Age (Ma)	Dis. (%)	* $\frac{^{207}\text{Pb}^*}{^{206}\text{Pb}^*}$	\pm (%)	* $\frac{^{206}\text{Pb}^*}{^{238}\text{U}}$	\pm (%)	err. corr.
GRS215-9.1	0,05	530	7	0,01	540 ± 8	533 ± 28	-1	0,05809	1,3	0,0874	1,5	0,8
GRS215-8.1	0,27	319	4	0,01	537 ± 8	521 ± 45	-3	0,05777	2,1	0,0868	1,5	0,6
GRS215-2.1	0,26	481	7	0,01	534 ± 8	534 ± 25	+0	0,05811	1,1	0,0864	1,6	0,8
GRS215-4.1	0,13	535	8	0,02	528 ± 7	519 ± 19	-2	0,05770	0,9	0,0854	1,4	0,9
GRS215-11.1	0,06	535	8	0,02	538 ± 9	512 ± 18	-5	0,05753	0,8	0,0870	1,7	0,9
GRS215-1.1	0,47	460	7	0,02	554 ± 8	553 ± 31	-0	0,05862	1,4	0,0897	1,6	0,7
GRS215-6.1	0,04	684	12	0,02	541 ± 7	532 ± 14	-2	0,05805	0,7	0,0876	1,4	0,9
GRS215-16.1	0,11	598	10	0,02	536 ± 7	550 ± 18	+3	0,05854	0,8	0,0867	1,4	0,9
GRS215-3.1	0,19	593	10	0,02	535 ± 7	546 ± 20	+2	0,05843	0,9	0,0865	1,4	0,8
GRS215-7.1	2,43	359	39	0,11	500 ± 7	515 ± 7	+3	0,05761	3,4	0,0806	1,5	0,4
GRS215-13.1	0,99	245	53	0,22	521 ± 7	660 ± 61	+22	0,06160	2,9	0,0842	1,5	0,5
GRS215-15.1	0,41	238	52	0,22	530 ± 9	580 ± 41	+9	0,05934	1,9	0,0857	1,8	0,7
GRS215-10.1	0,89	212	59	0,28	527 ± 8	614 ± 61	+15	0,06029	2,8	0,0852	1,5	0,5
GRS215-12.1	0,07	178	58	0,33	527 ± 8	639 ± 46	+18	0,06101	2,1	0,0852	1,5	0,6
GRS215-5.1	0,20	196	75	0,38	531 ± 8	585 ± 37	+10	0,05948	1,7	0,0859	1,5	0,7
GRS215-1.2	0,94	62	31	0,50	542 ± 9	550 ± 186	+1	0,05854	8,5	0,0877	1,8	0,2
GRS215-14.1	0,60	247	133	0,54	509 ± 14	481 ± 49	-6	0,05672	2,2	0,0821	2,8	0,8
GRS215-2.2	0,76	73	42	0,57	528 ± 9	512 ± 118	-3	0,05753	5,4	0,0854	1,7	0,3

Errors are 1-sigma; Pb_c and Pb* indicate the common and radiogenic portions, respectively.

Error in Standard calibration was 0.46% (not included in above errors but required when comparing data from different mounts).

* Common Pb corrected using measured ^{204}Pb .

laboratory staff using Iolite 3.32 software (Paton *et al.*, 2011; Paul *et al.*, 2012).

Sixty-eight zircon crystals from sample GRS-215, after SHRIMP acquisition, were analyzed by LA-ICP-MS. Some of them (nine) were rejected due to the presence of inclusions of apatite, fractures or compositional zoning. The selected zircon data are presented in Table 2 and 3, according to their Th/U ratio. This ratio, with discrepancies (Harley *et al.*, 2007), is used to discriminate between magmatic (Th/U>0,1) and metamorphic (Th/U<0,1) zircons (*e.g.* Hoskin and Schaltegger, 2003). However, examples of metamorphic zircon overgrowths with Th/U values higher than 0,1 (*e.g.* Carson *et al.*, 2002; Harley *et al.*, 2001; Hokada and Harley, 2004; Hu *et al.*, 2004; Kelly and Harley, 2005; Kröner *et al.*, 2000; Moller *et al.*, 2003; Pidgeon, 1992; Schaltegger *et al.*, 1999; Vavra *et al.*, 1999) or even igneous zircons with values lower than 0,1 have been referenced (Ladenberger *et al.*, 2014; Schärer,

1984; Sláma *et al.*, 2008; Zeck and Whitehouse, 1999). The extremely low Th/U ratio (\approx 0,01) in zircons is still considered a common discriminator of metamorphic zircons but the work of López-Sánchez *et al.* (2016), which describes magmatic zircon overgrowths with Th/U ratios (<0,02), questions its validity.

In this work, the Th/U ratio and the observed compositional zircon zonings can be apparently correlated with ZP₁ (low Th/U ratios from 0,01 to 0,1) and ZP₂ (high Th/U ratios, from 0,1 to 1) (Fig. 5A; Table 1), allowing to link them to a metamorphic or an igneous origin, respectively. However, due to its questionable validity, another geochemical parameter should be taken into account to link the zircons with their origin.

The Nb and Ta can also be used as discriminating elements between these two zircon populations, as ZP₂ have almost invariably higher Nb/Ta ratios than ZP₁ (Table 2, 3; Fig. 5B). When plotted in the Nb+Ta vs. Th+U diagram

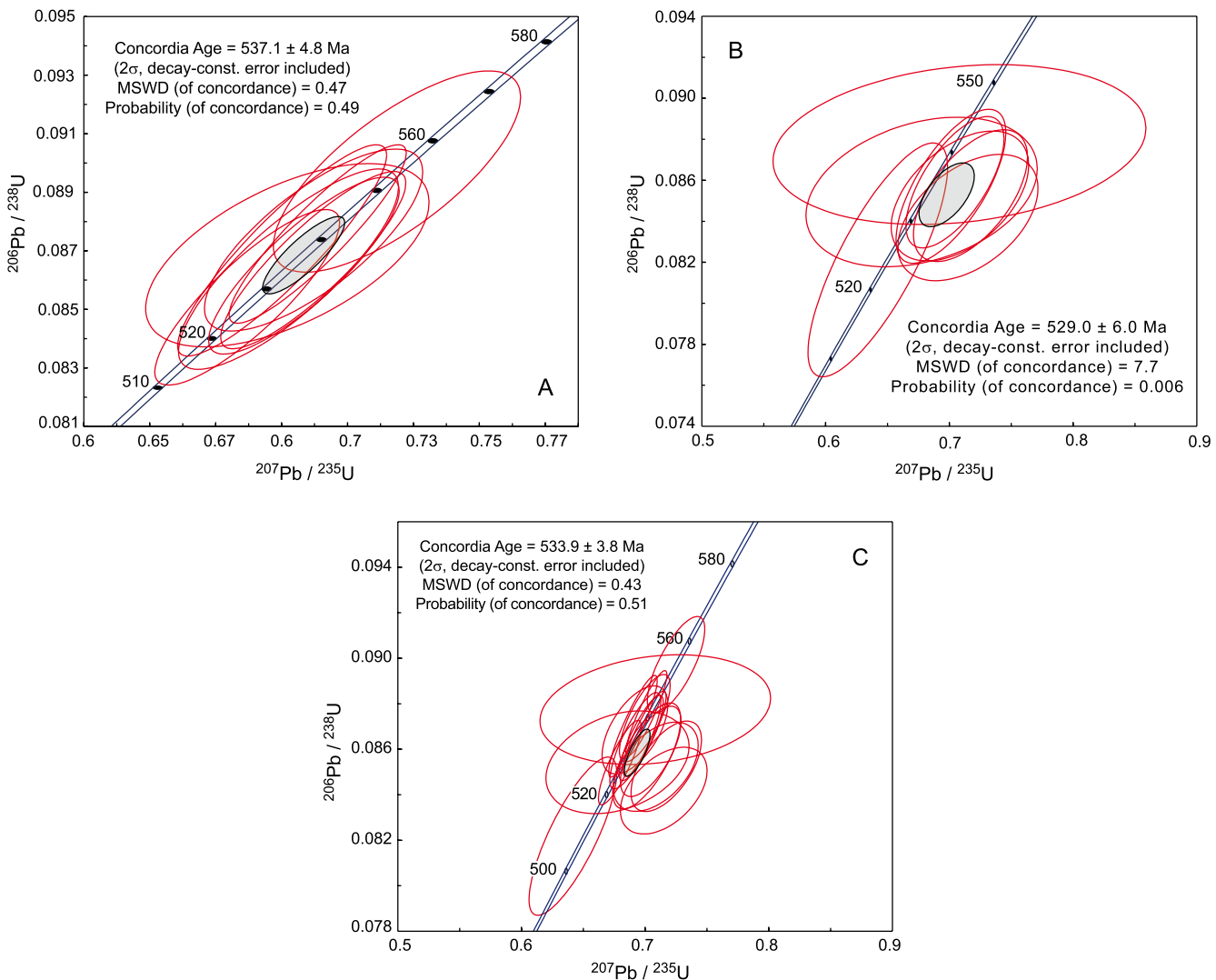


FIGURE 4. Wetherill Concordia plots of A) ZP₁ (metamorphic low Th/U zircons), B) ZP₂ (igneous high Th/U zircons) and C) both zircons populations together.

(Fig. 5C), a clear differentiation can be observed between the two zircon groups. ZP₂ zircons tend to plot towards higher Nb+Ta and lower Th+U values compared to ZP₁.

In general, it is assumed that zircons with a metamorphic origin have higher U and Hf and lower Ce concentrations than the igneous ones (*e.g.* Hoskin and Schaltegger, 2003). Moreover, the metamorphically grown zircons usually have flatter HREE (Heavy Rare Earth Elements) patterns, relatively low contents of HREE (and Y), and MREE (Middle Rare Earth Elements), low (Lu/Gd)_N, Nb/Ta, Y/Ho and Ce/Ce* ratios and high Eu/Eu* ratios than the igneous ones (*e.g.* Chen *et al.*, 2010).

The chondrite-normalized REE patterns (Sun and McDonough, 1989) of the analyzed zircons (Fig. 6) are

strongly enriched in HREE compared to LREE (Light Rare Earth Elements) and show prominent anomalies in Ce (positive) and Eu (negative). The ranges of normalized REE patterns of both zircon populations overlap (Fig. 6), but differ from normalized trends for the HREE. The ZP₁ zircons have flat HREE patterns [(Lu/Gd)_N ratios up to 10] whereas ZP₂ shows steeper patterns [(Lu/Gd)_N ratios up to 46]. In the LREE, MREE or HREE vs. Th/U plots (Fig. 5D-F) the REE contents do not show significant variations but increases slightly as the Th/U increases in ZP₂.

In the Th/U vs. Hf plot (Fig. 5G), the Hf concentration decreases from ZP₁ to ZP₂. The U/Ce vs. Th/U or Th plots can be considered as potential indicators of metamorphic and igneous zircons since

TABLE 2. Laser ablation trace, REE, and calculated temperature data for analyzed metamorphic zircons (ZP_1) from Río de los Sauces. In ppm. <dl: under detection limit

Sample	GRS_215																						
Source file	59	36	64	24	50	11	43	55	34	62	30	57	14	28	67	12	10	8	66	21	51	20	
P	742	698	1060	1096	836	909	1004	785	716	1016	813	1113	921	1097	927	1041	1568	760	707	923	681	679	
Sc	380	389	511	519	430	455	455	412	430	484	453	510	446	491	446	477	740	433	372	458	380	418	
Ti	3.6	4.3	3.6	4.3	3.9	4.1	3.8	3.8	4.4	3.7	4.4	4.2	4.2	6.3	3.9	4.7	6.0	4.8	4.0	5.0	3.7	4.4	
V	8.3	3.1	0.5	0.5	3.2	0.2	0.4	1.1	7.9	< dl	1.4	1.2	1.9	11.7	3.4	5.7	27.5	3.3	2.2	7.2	< dl	2.4	
Mn	4.3	3.2	0.4	2.9	3.3	< dl	0.5	2.8	33.0	0.5	39.0	1.6	0.9	16.7	1.8	2.3	26.7	21.3	2.8	4.2	< dl	5.3	
Fe	44.0	250	< dl	23.0	31.2	5.5	< dl	0.5	14.0	520	< dl	39.1	47.0	6.6	1120	22.0	30.0	515	374.0	250	107	4.8	11.0
Ga	< dl	0.27	< dl	0.22	< dl	< dl	< dl	< dl	0.56	< dl	0.34	< dl	< dl	0.54	0.17	0.32	1.46	0.59	0.44	0.40	< dl	0.18	
Sr	0.90	1.20	0.21	1.65	1.14	0.22	0.25	1.13	2.02	0.25	1.89	0.87	0.57	2.29	0.79	1.32	7.62	1.41	0.81	2.04	< dl	0.77	
Y	859	849	1405	1465	1146	1247	1430	1059	923	1421	1020	1633	1264	1475	1237	1378	1941	961	801	1220	917	1123	
Nb	1.4	1.6	2.2	2.1	1.9	2.4	2.5	1.7	1.7	2.2	1.9	2.3	2.6	2.6	1.9	2.7	2.9	2.0	1.4	2.2	1.9	1.8	
Sn	0.6	0.5	0.5	0.7	0.6	0.6	0.6	0.5	0.5	0.6	0.5	0.7	0.7	0.8	0.5	0.7	1.1	0.7	0.7	0.5	0.6		
Ba	3.7	2.2	0.1	1.7	3.4	< dl	0.2	1.6	6.0	0.3	6.3	2.1	1.0	8.3	2.4	3.2	21.8	8.1	2.6	5.5	< dl	2.0	
La	1.3	0.8	0.1	0.9	1.6	< dl	0.1	0.7	1.3	0.2	1.5	1.0	0.6	2.1	1.1	1.8	8.0	1.0	0.9	1.9	< dl	0.8	
Ce	10.7	6.1	0.7	8.2	7.3	0.9	1.5	4.4	7.5	1.9	14.1	8.2	4.3	14.6	7.2	11.7	41.7	6.1	7.8	14.4	3.2	7.8	
Pr	1.0	1.2	0.1	1.5	1.0	< dl	0.1	0.7	1.4	0.2	3.2	1.2	0.7	2.4	1.1	1.5	6.1	1.1	1.2	2.5	< dl	0.9	
Nd	5.1	7.8	0.9	10.8	5.8	0.9	1.3	4.5	8.0	1.9	22.9	7.3	4.4	14.1	6.0	9.1	32.4	6.6	6.0	15.9	1.0	5.5	
Sm	4.1	5.7	4.6	10.3	5.4	4.5	4.9	4.7	5.6	5.2	20.2	8.4	5.7	10.1	6.2	7.9	18.5	4.9	5.7	12.6	3.7	5.8	
Eu	1.6	2.0	0.4	2.4	1.7	0.4	0.5	1.6	2.1	0.5	4.3	2.6	1.4	4.0	1.7	3.2	8.0	1.6	1.3	3.7	0.4	2.0	
Gd	25.9	23.5	43.9	51.3	35.8	38.4	43.9	30.9	26.8	44.9	50.3	54.4	40.4	49.8	39.5	44.6	57.8	26.0	26.4	44.3	27.9	32.6	
Tb	11.3	10.7	19.9	20.7	15.8	17.7	20.0	13.8	12.1	20.2	16.9	23.7	18.9	20.8	16.9	20.3	24.6	11.6	11.0	17.4	11.6	13.3	
Dy	123	116	213	220	172	191	222	151	137	213	162	251	199	224	180	211	290	139	120	180	122	147	
Ho	29	29	49	51	40	44	49	37	33	48	36	59	45	52	42	48	74	33	27	42	30	38	
Er	88	94	144	156	122	131	147	117	110	144	107	179	137	162	131	147	265	110	83	130	95	135	
Tm	15	17	25	27	21	23	25	22	22	25	18	31	24	28	23	26	53	20	15	23	17	25	
Yb	119	133	190	195	162	175	183	186	179	193	139	239	189	210	175	203	462	157	108	175	132	196	
Lu	18	20	31	32	27	26	29	29	26	31	22	37	27	34	28	29	71	24	18	27	20	31	
Hf	12130	13130	11820	11740	12120	11310	11590	11850	12290	11550	12680	11700	11970	11740	12040	11700	12520	12620	12700	12090	11520	12070	
Ta	1.4	1.5	1.8	1.8	2.1	2.0	1.9	1.6	1.6	2.0	1.6	2.2	2.2	2.1	1.8	2.4	3.3	1.7	1.3	1.9	1.5	1.4	
Pb	238	234	275	296	244	318	374	244	211	285	270	318	342	321	248	359	297	231	204	271	213	176	
Th	8.5	9.0	11.7	12.1	11.1	14.7	16.6	11.0	11.1	12.9	11.1	15.8	18.4	17.2	13.2	21.8	22.3	17.5	16.9	37.8	34.4	31.1	
U	571	537	655	681	615	782	880	572	576	650	541	766	870	772	589	905	877	588	459	686	493	425	
REE	453	467	722	785	618	652	728	603	571	729	618	903	697	826	660	764	1412	541	430	689	464	641	
Th/U	-	0.02	0.02	0.02	0.02	0.02	0.02	0.02	0.02	0.02	0.02	0.02	0.02	0.02	0.02	0.02	0.03	0.03	0.04	0.06	0.07	0.07	
Nb/Ta	1.0	1.1	1.2	1.2	1.0	1.1	1.2	0.9	1.1	1.1	1.1	1.0	1.2	1.3	1.1	1.1	0.9	1.2	1.1	1.1	1.3	1.3	
T (°C)	715	731	716	731	724	727	720	721	733	719	735	729	768	723	741	762	741	725	745	719	735		

the magmatic zircons show little variation in U/Ce while the metamorphic ones are enriched in U due to increase in water content during dehydration reactions (Castiñeiras *et al.*, 2011). In our study, the analyzed zircons are again split into two main populations: ZP_2 is characterized by high Th and little variation in the U/Ce content, and the ZP_1 by low Th and highly variable U/Ce contents (Fig. 5H). The application of Grimes *et al.* (2007) diagrams agrees with zircons evolved from a continental crust (Fig. 7).

Ti-IN-ZIRCON GEOTHERMOMETRY

The Ti-in-zircon content was used to calculate the approximate crystallization temperatures of the metamorphic and igneous zircons using the equation of Ferry and Watson (2007). As the studied samples are saturated in SiO_2 ($a_{\text{SiO}_2}=1$), rutile is absent ($a_{\text{TiO}_2}<1$) but titanite is present ($a_{\text{TiO}_2}>0.5$), we have applied values of $a_{\text{SiO}_2}=1$ and $a_{\text{TiO}_2}=0.5$ to calculate the crystallization temperatures (Table 2; 3). Mean temperatures of 735 ± 17 and $750 \pm 22^\circ\text{C}$ were obtained for the metamorphic (4.5ppm Ti) and igneous (5.5ppm Ti) zircons, respectively. The calculated temperatures are within the uncertainty of each other, although a slight increase towards the igneous zircons is predicted (Fig. 5I).

DISCUSSION

The zircons from the Río de los Sauces granite yielded uncommon geochemical signatures and SHRIMP results. The following results stand out twofold as i) two zircon populations (ZP_1 and ZP_2) with different textures and geochemical signatures and ii) a bimodal age distribution in the geochemical two end-members, 537 ± 4.8 and $529 \pm 6\text{Ma}$, have been identified. According to presented geochemical features, zircon textural analysis and Ti-in-zircon geothermometry we proposed that the identified ZP_1 and ZP_2 can be correlated with metamorphic and igneous zircons populations respectively, and do confirm the utility of the Th/U, U/Ce and Nb/Ta as potential ratios for zircon nature indicator. These new data aid in the understanding of the metamorphic evolution of the Calamuchita complex migmatites and help to constrain the time gap between the Pampean HT metamorphism and the crystallization of anatectic granites.

Melting products forming leucosomes in migmatites are commonly related to the formation of sheets like bodies of leucogranites and larger accumulations of magmatic rocks along the Sierra de Comechingones as leucosomes are texturally and compositionally similar to the leucogranitic bodies (Barzola *et al.*, 2019). The Río de los Sauces granite is a sheeted intrusion emplaced into

TABLE 3. Laser ablation trace, REE and calculated temperature data for analyzed igneous zircons (ZP_2) from Río de los Sauces. In ppm. <dl: under detection limit

Sample	GRS_215																					
Source file	32	29	25	60	68	63	17	52	40	56	6	37	46	35	49	61	31	58	23	48	9	19
P	1174	1510	612	642	866	1390	469	830	822	920	396	342	980	402	1070	490	630	958	772	920	875	434
Sc	508	576	392.1	382	423	473	366	519	387	419	362.5	328.1	393	337.6	423	358	386.5	404	406	382.5	432	356.6
Ti	4.8	6.6	3.9	4.5	4.8	5.7	4.6	4.6	5.1	4.2	4.8	4.0	4.5	4.4	5.0	4.3	5.1	6.0	5.3	5.0	5.4	6.4
V	24.3	37.4	< dl	14.4	4.8	58.0	2.1	11.5	15.2	8.3	0.9	< dl	6.2	< dl	11.0	0.5	1.4	3.3	3.6	3.3	10.4	< dl
Mn	49.0	27.1	< dl	4.9	2.3	17.6	1.8	8.6	3.6	6.1	0.7	< dl	2.7	< dl	7.2	2.7	1.5	3.8	5.4	15.9	3.8	4.2
Fe	84.4	269.0	< dl	376.0	23.5	200.0	38.0	660.0	65.0	48.0	52.0	< dl	22.9	< dl	391.0	129.0	20.9	28.4	73.0	940.0	173.0	126.0
Ga	0.60	1.76	< dl	0.36	0.34	0.85	0.32	0.62	0.36	0.44	0.28	< dl	< dl	< dl	0.75	0.60	0.35	0.45	0.55	0.69	0.73	0.53
Sr	2.64	8.20	0.22	1.90	1.81	6.10	0.86	2.50	1.74	1.65	0.51	0.16	0.83	0.12	3.27	0.38	0.34	1.99	1.76	0.51	1.45	0.97
Y	1402	1960	906	860	1286	2223	697	1200	1141	1337	523	493	1820	489.5	1690	637	1043	1377	1190	1510	1650	544
Nb	2.9	2.7	2.8	3.1	3.5	2.1	2.4	2.3	2.8	2.1	2.0	2.5	2.0	2.5	1.8	2.3	2.0	2.5	1.9	3.3	2.0	
Sn	0.8	0.9	0.7	< dl	0.8	1.0	0.8	1.0	0.5	0.7	0.7	0.5	0.4	0.5	0.7	0.7	0.7	0.8	0.4	0.5	0.8	
Ba	11.7	32.7	< dl	6.7	6.3	23.3	2.7	7.2	7.4	5.9	1.1	< dl	2.2	< dl	11.4	0.8	1.4	5.7	17.0	0.6	6.0	0.4
La	5.3	14.3	< dl	3.0	2.5	13.8	0.8	4.0	4.6	3.8	0.4	< dl	1.6	< dl	5.2	0.1	0.4	2.7	1.4	0.3	4.1	< dl
Ce	20.6	88.0	6.2	23.0	25.5	47.2	15.7	29.0	25.0	29.7	11.8	10.1	12.7	8.8	40.0	11.2	11.9	23.1	18.6	9.8	27.6	12.0
Pr	2.8	12.4	0.1	2.0	2.8	6.5	1.1	3.0	2.6	2.9	0.6	0.1	1.1	0.1	4.2	0.2	0.6	2.7	1.6	0.4	2.5	0.2
Nd	16.6	67.0	1.4	10.8	17.6	36.8	7.2	19.1	15.9	16.6	5.4	1.7	10.5	1.6	22.7	3.0	7.0	18.0	12.3	5.9	14.7	5.0
Sm	12.5	33.2	4.9	8.8	13.8	26.2	7.7	18.6	10.8	13.4	6.2	4.8	14.2	4.4	19.6	6.2	13.1	17.0	13.3	11.6	14.8	12.5
Eu	6.1	16.2	0.7	4.8	4.8	9.3	2.2	6.0	5.6	4.9	1.4	0.7	3.5	0.6	6.5	1.4	2.2	5.4	3.7	2.0	5.2	1.7
Gd	48.3	78.0	29.2	33.9	52.1	93.5	30.7	66.4	41.3	52.4	25.7	24.9	68.0	23.8	74.7	28.1	57.2	62.2	47.7	55.9	58.0	48.9
Tb	16.0	26.2	9.5	10.3	15.7	27.7	9.3	18.6	12.5	16.0	7.6	7.2	21.0	7.0	20.7	7.9	15.6	17.8	13.5	16.6	17.7	12.0
Dy	175	284	106	110	163	287	90	180	142	169	73	69	237	65	218	79	144	183	145	184	204	93
Ho	51	74	31	29	45	81	23	44	44	52	18	17	71	17	64	23	36	53	44	56	64	19
Er	204	256	121	100	171	314	82	145	176	203	59	51	263	57	255	87	121	193	173	223	267	51
Tm	42	48	24	18	32	64	15	25	36	41	10	8	49	10	51	18	20	35	33	43	53	7
Yb	361	376	186	144	242	519	112	192	297	339	73	60	365	74	417	150	149	272	266	342	445	51
Lu	55	55	31	22	40	81	17	25	48	54	10	8	62	11	69	27	22	43	46	59	73	7
Hf	12620	12410	12140	12260	11590	11680	11370	10870	10680	11960	11520	11430	11630	11110	10210	11170	10490	10010	10060	9820	10780	11400
Ta	1.8	1.7	1.8	1.9	1.9	2.3	1.3	1.3	1.5	1.8	1.3	1.3	2.0	1.2	3.2	1.1	1.2	1.0	1.3	1.1	1.7	1.0
Pb	215	275	146	150	144	216	95	143	82	138	79	88	165	75	106	62	90	56	63	73	119	57
Th	80	166	64	87	95	166	83	148	69	117	71	82	154	71	154	72	109	77	87	95	192	82
U	489	920	336	354	367	624	243	433	199	331	198	210	392	163	339	149	214	148	165	160	320	136
REE	1017	1429	551	520	827	1606	413	775	862	998	302	262	1179	281	1268	442	600	927	818	1010	1251	320
Th/U	0.16	0.18	0.19	0.25	0.26	0.27	0.34	0.34	0.35	0.35	0.36	0.39	0.39	0.44	0.45	0.48	0.51	0.52	0.53	0.59	0.60	0.60
Nb/Ta	1.60	1.57	1.50	1.48	1.64	1.52	1.59	1.85	1.48	1.56	1.64	1.51	1.26	1.65	0.78	1.61	1.92	2.03	1.93	1.65	1.89	2.05
T (°C)	742	773	724	736	742	758	739	737	748	731	742	726	735	734	745	732	747	762	752	746	752	770

gneisses related to anatetic melt during the migmatization and can be considered as a syn- to the late-M₂ body. In this regard, the age of 529±6 Ma obtained from high Th/U (ZP_2) zircons is interpreted as the crystallization age of the Río de los Sauces granite, and therefore it dates the vanishing stages of M₂. Meanwhile, the age of 537±5 Ma, obtained from low Th/U (ZP_1) metamorphic zircons, could represent the age of the Pampean HT metamorphism prior to the anatexis. This metamorphic event might be the origin of the solid-state growth of metamorphic zircons, which were further incorporated in the melts without dissolving until newly crystallization of igneous ones at the age of 529±6 Ma. This age agrees well with the previously published ages for the Pampean metamorphism in other parts of the Sierras de Córdoba (Guereschi and Martino, 2014; and references therein).

Although the temporal relationship between the metamorphism and the anatexis differ from orogen to orogen, time gaps of less than 10 Myr between the syntectonic granites and regional metamorphism have been reported in other orogenic domains. For example, in the island of Naxos (Greece), a time lag of at least 5 Myr between the peak of the Miocene metamorphism and the main period of magmatism was reported by Keay *et al.* (2001). While, a time span of 7 Myr, has been established by Esteban *et al.* (2015) between the metamorphic

climax of the HT/LP Variscan metamorphism (Late Carboniferous) and the final emplacement of the Lys-Caillouas pluton (Late Carboniferous–Early Permian) at middle crustal levels. The latter geochronological study presents many similarities with our study because in both cases zircons from only one granite body have been sufficient to detect the time gap between the two processes.

The presence of zircons with metamorphic affinity in the Río de los Sauces granite suggests the incomplete assimilation of the zircons derived from the metamorphic protoliths and opens an opportunity to study the timing of the metamorphism prior to the emplacement of the pluton. The mean temperatures of 735±17 and 750±22°C determined by Ti-in-zircon in metamorphic and igneous zircons, respectively, are, although slightly lower, coherent to the calculated metamorphic conditions in the Sierras de Córdoba (Fagiano, 2007; Otamendi *et al.*, 2004; Rapela *et al.*, 1998). Since the crystallization temperatures calculated for igneous and metamorphic zircons are within the uncertainty of each other, a further increase in the regional temperature during anatexis cannot be inferred. Finally, the age of the climax of the Pampean metamorphism has been constrained between 537 and 529 Ma, and the Concordia age of 534±4 (2σ) Ma,

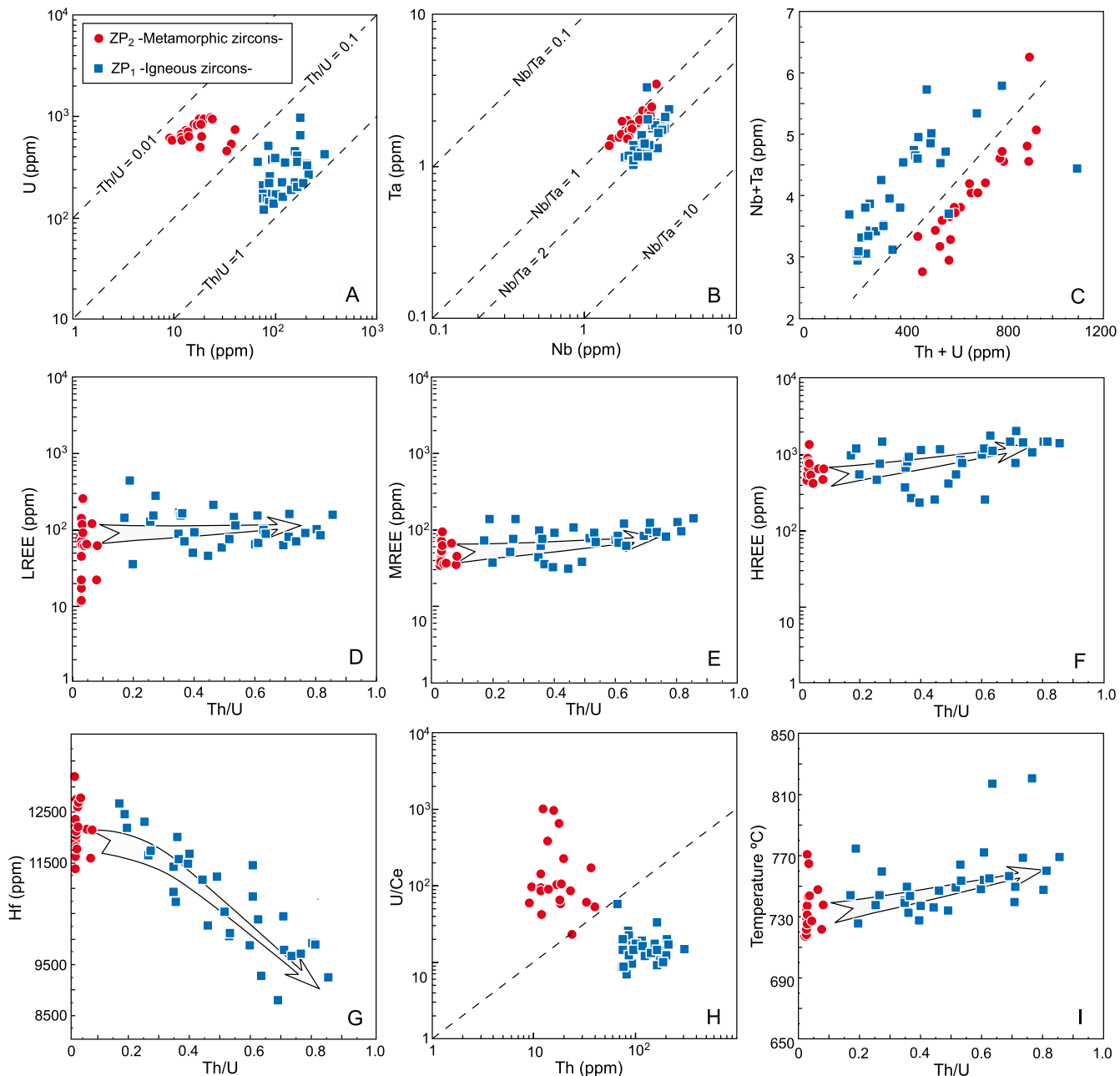


FIGURE 5. Bivariate diagrams with contrasting trace and REE concentrations of both zircon populations (metamorphic-ZP₁ and igneous-ZP₂). A) Th vs. U; B) Nb vs. Ta; C) U+Th vs. Nb+Ta; D, E, F) Th/U vs. LREE, MREE and HREE, respectively; G) Th/U vs. Hf; H) Th vs. U/Ce; I) Th/U vs. temperature.

obtained from both types of zircons, has been considered as the mean age of the HT Pampean metamorphism in the Sierras de Córdoba.

CONCLUSIONS

The presence of zircons with metamorphic and igneous affinities in the Río de los Sauces granite,

identified by LA-ICP-MS analyses, suggest their incomplete assimilation during the anatexis and open the opportunity to date both processes from the same sample.

U-Pb SHRIMP analyses from both kind of zircons suggest that the Río de los Sauces granite crystallized at 529 ± 6 (2σ) Ma, whereas the age of 537.1 ± 4.8 (2σ) Ma refers to the Pampean metamorphism prior to the

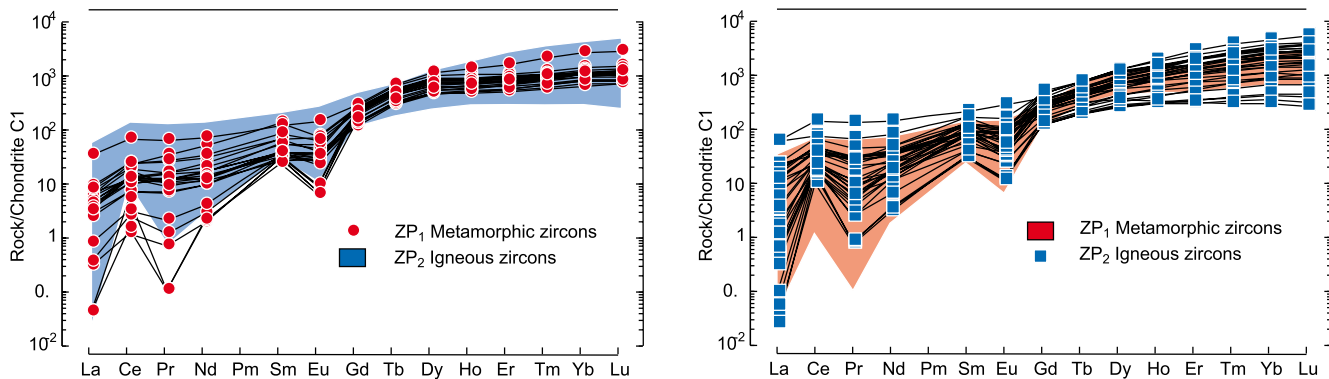


FIGURE 6. Chondrite-normalized (Sun and McDonough, 1989) REE patterns of both zircon populations (ZP₁ and ZP₂).

emplacement of the pluton, and could be considered as a good approximation for the Pampean HT metamorphism of the study area.

A time gap of ≈ 8 Myr is established between the metamorphism and the granite crystallization.

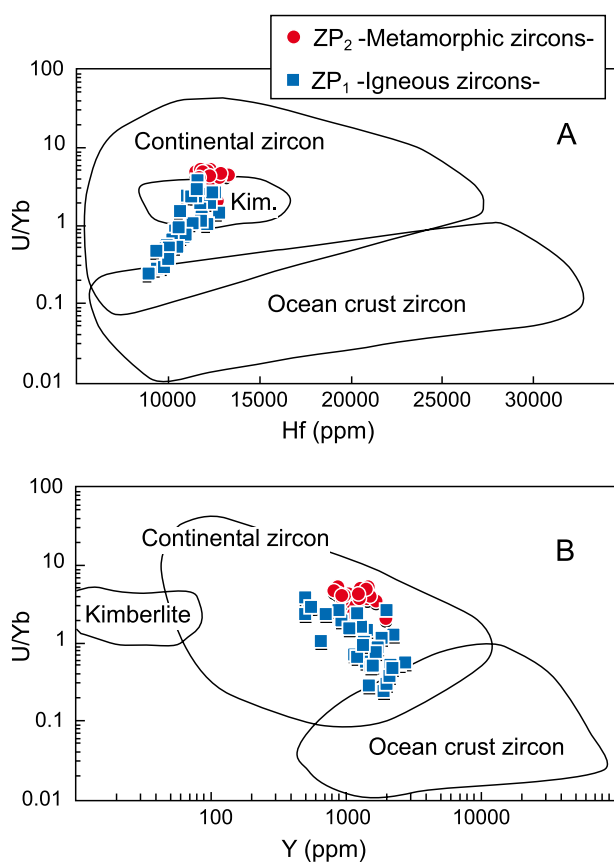


FIGURE 7. A) U/Yb vs. Hf and B) U/Yb vs. Y plots of both zircon populations (metamorphic-ZP₁ and igneous-ZP₂). The fields for continental and oceanic crust zircons are from Grimes *et al.* (2007).

The Ti-in-zircon geothermometry yielded temperatures of *ca.* 750±22°C for the granite crystallization and thus constrain the minimum temperature reached during the anatexis.

According to obtained and previously published data, we suggest that LA-ICP-MS and U-Th-Pb SHRIMP analyses should be performed together in order to achieve a well geochemical zircon characterization, previous to the granitoid dating.

The Th/U, U/Ce and Nb/Ta ratios can be considered as very useful markers to infer the igneous or metamorphic nature of the zircons.

ACKNOWLEDGMENTS

This work has been supported by grants PICT1754/16, PIP688 CONICET, GIU17/033 of “Grupos de Investigación” of the University of the Basque Country, and CGL2017-82976-P (Ministerio de Economía, Industria y Competitividad/Agenzia Estatal de Investigación/Fondo Europeo de Desarrollo Regional, European Union). We thank Gloria Gallastegui and an anonymous reviewer for their very constructive suggestions that significantly improved the manuscript.

REFERENCES

- Aceñolaza, EG., Aceñolaza, E., 2007. Insights in the Neoproterozoic-Early Cambrian transition of NW Argentina: facies, environments and fossils in the proto-margin of western Gondwana. In: Vickers-Rich, P., Komarower, P. (eds.). *The Rise and Fall of the Ediacaran Biota*. London, Geological Society, 286 (Special Publications), 1-13.
- Aceñolaza, FG., Toselli, A., 2009. The Pampean Orogen: Ediacaran-Lower Cambrian evolutionary history of Central and Northwest region of Argentina. In: Gaucher, C., Sial,

- A.N., Halverson, G.P., Frimmel, H.E. (eds.). Neoproterozoic-Cambrian Tectonics, Global Change and Evolution: a focus on southwestern Gondwana. *Developments in Precambrian Geology*, 16, 239-254.
- Barzola, M.G., Tibaldi A.M., Cristofolini, E.A., Otamendi, J.E., Demichelis, A.H., Armas, P., Camilletti, G.C., 2019. Estructura interna de una sección de corteza media expuesta en el basamento metamórfico del sector centro-norte de sierra de Comechingones, Córdoba. *Revista de la Asociación Geológica Argentina*, 76(4), 375-390.
- Black, L.P., Kamo, S.L., Allen, C.M., Davis, D.W., Alenikoff, J.N., Valley, J.W., Mundif, R., Campbell, I.H., Korsch, R.J., Williams, I.S., Foudoulis, C., 2004. Improved $^{206}\text{Pb}/^{238}\text{U}$ microprobe geochronology by the monitoring of trace element related matrix effect; SHRIMP ID-TIMS, ELA-ICP-MS and oxygen isotope documentation for a series of zircon standards. *Chemical Geology*, 205(1), 115-140.
- Carson, C.J., Ague, J.J., Grove, M., Coath, C.D., Harrison, T.M., 2002. U-Pb geochronology from Tonagh Island, East Antarctica: implications for the timing of ultra-high temperature metamorphism in the Napier Complex. *Precambrian Research*, 116, 237-263.
- Casquet, C., Dahlquist, J.A., Verdecchia, S.O., Baldo, E.G., Galindo, C., Rapela, C.W., Pankhurst, R.J., Morales, M.M., Murra, J.A., Fanning, C.M., 2018. Review of the Cambrian Pampean orogeny of Argentina; a displaced orogen formerly attached to the Saldania Belt of South Africa? *Earth-Science Reviews*, 177, 209-225.
- Castiñeiras, P., Navidad, M., Casas, J.M., Liesa, M., Carreras, J., 2011. Petrogenesis of Ordovician magmatism in the Pyrenees (Albera and Canigó Massifs) determined on the basis of zircon minor and trace element composition. *Journal of Geology*, 119, 521-34.
- Cawood, P.A., 2005. Terra Australis Orogen: Rodinia breakup and development of the Pacific and Iapetus margins of Gondwana during the Neoproterozoic and Paleozoic. *Earth-Science Reviews*, 69, 249-279.
- Chen, R-X., Zheng, Y.F., Xie, L., 2010. Metamorphic growth and recrystallization of zircon: Distinction by simultaneous in-situ analyses of trace elements, U-Th-Pb and Lu-Hf isotopes in zircons from eclogite-facies rocks in the Sulu orogen. *Lithos*, 114, 132-154.
- Dahlquist, J.A., Verdecchia, S.O., Baldo, E.G., Basei, M.A.S., Alasino, P.H., Urán, G.A., Rapela, C.W., Da Costa Campos Neto, M., Zandomeni, P.S., 2016. Early Cambrian U-Pb zircon age and Hf-isotope data from the Guasayán pluton, Sierras Pampeanas, Argentina: implications for the northwestern boundary of the Pampean arc. *Andean Geology*, 43(1), 137-150.
- Escayola, M.P., Pimentel, M.M., Armstrong, R., 2007. Neoproterozoic back arc basin: sensitive high-resolution ion microprobe U-Pb and Sm-Nd isotopic evidence from eastern Pampean ranges, Argentina. *Geology*, 35, 495-498.
- Esteban, J.J., Aranguren, A., Cuevas, J., Hilario, A., Tubía, J.M., Larionov, A., Sergeev, S., 2015. Is there a time lag between the metamorphism and emplacement of plutons in the Axial Zone of the Pyrenees? *Geological Magazine*, 152, 935-941.
- Fagiano, M., 2007. Geología y Petrología del basamento cristalino de las Albahacas, sur de la Sierra de Comechingones, Córdoba. PhD Thesis. Río Cuarto, Universidad Nacional de Río Cuarto, 380pp.
- Ferry, J.M., Watson, E.B., 2007. New thermodynamic models and revised calibrations for the Ti-in-zircon and Zr-in-rutile thermometers. *Contributions to Mineralogy and Petrology*, 154, 429-37.
- Grimes, C.B., John, B.E., Kelemen, P.B., Mazdab, F.K., Wooden, J.L., Cheadle, M.J., Hanghøj, K., Schwartz, J.J., 2007. Trace element chemistry of zircons from oceanic crust: a method for distinguishing detrital zircon provenance. *Geology*, 35, 643-6.
- Guereschi, A.B., Martino, R.D., 2014. Las migmatitas de las Sierras de Córdoba. In: Martino, R.D., Guereschi, A.B. (eds.). Relatorio del XIX congreso geológico argentino: geología y recursos naturales de la provincia de Córdoba. Asociación Geológica Argentina, 125-148.
- Harley, S.L., Kinny, P.D., Snape, I., Black, L.P., 2001. Zircon chemistry and the definition of events in Archaean granulite terrains. In: Cassidy, K.F., Dunphy, J.M., van Kranendonk, M.J. (eds.). Extended abstracts of the 4th International Archaean Symposium. Canberra, AGSO-Geoscience Australia Record 2001/37, 511-513.
- Harley, S.L., Kelly, N.M., Möller, A., 2007. Zircon behaviour and the thermal histories of mountain chains. *Elements*, 3, 25-30.
- Hauser, N., Matteini, M., Omarini, R.H., Piementel, M.M., 2011. Combined U-Pb and Lu-Hf isotope data on turbidites of the Paleozoic basement of NW Argentina and petrology of associated igneous rocks: Implications for the tectonic evolution of western Gondwana between 560 and 460 Ma. *Gondwana Research*, 19(1), 100-127.
- Hokada, T., Harley, S.L., 2004. Zircon growth in UHT leucosome: constraints from zircon-garnet rare earth elements (REE) relations in Napier Complex, East Antarctica. *Journal of Mineralogical and Petrological Sciences*, 99, 180-190.
- Hoskin, P.W.O., Schaltegger, U., 2003. The composition of zircon and igneous and metamorphic petrogenesis. *Reviews in Mineralogy and Geochemistry*, 53(1), 27-55.
- Hu, F.F., Fan, H.R., Yang, J.H., Wan, Y.S., Liu, D.Y., Zhai, M.G., Jin, C.W., 2004. Mineralizing age of the Rushan lode gold deposit in the Jiaodong Peninsula: SHRIMP U-Pb dating on hydrothermal zircon. *Chinese Science Bulletin*, 49, 1629-1636.
- Iannizzotto, N.E., Rapela, C.W., Baldo, E.G., Galindo, C., Fanning, C.M., 2013. The Sierra Norte-Ambargasta Batholith: Cambrian magmatism formed in a transpressional belt along the western edge of the Río de la Plata cratón? *Journal of South American Earth Sciences*, 42, 127-142.
- Ježek, P., Willner, A.P., Aceñolaza, F.G., Miller, H., 1985. The Puncoviscana trough - a large basin of Late Precambrian to Early Cambrian age on the Pacific edge of the Brazilian shield. *Geologische Rundschau*, 74(3), 573-584.
- Jochum, K.P., Weis, U., Stoll, B., Kuzmin, D., Yang, Q., Raczek, I., Jacob, D.E., Stracke, A., Birbaum, K., Frick, D.A., Günther, D., Enzweiler, J., 2011. Determination of reference values

- for NIST SRM 610–617 glasses following ISO guideline. *Geostandards and Geoanalytical Research*, 35, 397–429.
- Keay, S., Lister, G., Buick, I., 2001. The timing of partial melting, Barrovian metamorphism and granite intrusion in the Naxos metamorphic core complex, Cyclades, Aegean Sea, Greece. *Tectonophysics*, 342, 275–312.
- Kelly, N.M., Harley, S.L., 2005. An integrated microtextural and chemical approach to zircon geochronology: Refining the Archaean history of the Napier Complex, east Antarctica. *Contributions to Mineralogy and Petrology*, 149, 57–84.
- Kröner, A., O'Brian P.J., Nemchin, A.A., Pidgeon, R.T., 2000. Zircon ages for high pressure granulites from South Bohemia, Czech Republic, and their connection to Carboniferous high temperature processes. *Contributions to Mineralogy and Petrology*, 138, 127–142.
- Ladenberger, A., Be'eri-Shlevin, Y., Claesson, S., Gee, D.G., Majka, J., Romanova, I.V., 2014. Tectonometamorphic evolution of the Areskutan Nappe – Caledonian history revealed by SIMS U–Pb zircon geochronology. In: Corfu, F., Gasser, D., Chew, D.M. (eds.). *New Perspectives on the Caledonides of Scandinavia and Related Areas*. London, Geological Society, 390 (Special Publications), 337–368.
- Lira, R., Millone, H.A., Kirschbaum, A.M., Moreno, R.S., 1997. Calc-alkaline arc granitoid activity in the Sierra Norte-Ambargasta ranges, central Argentina. *Journal of South American Earth Sciences*, 10(2), 157–177.
- López-Sánchez, M.A., Aleinikoff, J.N., Marcos, A., Martínez, E.J., Llana-Fúnez, S., 2016. An example of low-Th/U zircon overgrowths of magmatic origin in a late orogenic Variscan intrusion: the San Ciprián massif (NW Spain). London, The Geological Society, 173(2), 282–291.
- Ludwig, K.R., 2003. User's Manual for Isoplot/Ex, Version 3.00: A Geochronological Toolkit for Microsoft Excel. Berkeley Geochronology Center, 4 (Special Publication), 73pp.
- Martino, R.D., Guereschi, A.B., 2014. La estructura neoproterozoica-paleozoica inferior del complejo metamórfico de las Sierras Pampeanas de Córdoba. In: Martino, R.D., Guereschi, A.B. (eds.). *Relatorio del XIX congreso geológico argentino: geología y recursos naturales de la provincia de Córdoba*. Asociación Geológica Argentina, 95–128.
- Moller, A., O'Brien, P.J., Kennedy, A., Kröner, A., 2003. Linking growth episodes of zircon and metamorphic textures to zircon chemistry: An example from the ultrahigh-temperature granulites of Rogaland (SW Norway). In: Vance, D., Müller, W., Villa, I.M. (eds.). *Geochronology: Linking the Isotopic Record with Petrology and Textures*. London, Geological Society, 220 (Special Publications), 65–81.
- Omarini, R.H., Sureda, R.J., Götz, H.J., Seilacher, A., Pfleiderer, F., 1999. Puncoviscana folded belt in northwestern Argentina: testimony of late Proterozoic Rodinia fragmentation and pre-Gondwana collisional episodes. *International Journal of Earth Science*, 88(1), 76–97.
- Otamendi, J.E., Castellarini, P.A., Fagiano, M., Demichelis, A., Tibaldi, A., 2004. Cambrian to Devonian geologic evolution of the Sierra de Comechingones, eastern Sierras Pampeanas: evidence for the development and exhumation of continental crust on the proto-pacific margin of Gondwana. *Gondwana Research*, 7(4), 1143–1155.
- Paton, C., Hellstrom, J., Paul, B., Woodhead, J., Hergt, J., 2011. Iolite: freeware for the visualization and processing of mass spectrometric data. *Journal of Analytical Atomic Spectrometry*, 26, 2508–2518.
- Paul, B., Paton, C., Norris, A., Woodhead, J., Hellstrom, J., Hergt, J., Greig, A., 2012. CellSpace: a module for creating spatially registered laser ablation images within the Iolite freeware environment. *Journal of Analytical Atomic Spectrometry*, 27, 700–706.
- Pidgeon, R.T., 1992. Recrystallisation of oscillatory zoned zircon: Some geochronological and petrological implications. *Contributions to Mineralogy and Petrology*, 110, 463–472.
- Rapela, C.W., Pankhurst R.J., Casquet, C., Baldo, E., Saavedra, J., Galindo, C., Fanning, C.M., 1998. The Pampean orogeny of the southern proto-Andes: Cambrian continental collision in the Sierras de Córdoba. In: Pankhurst, R.J., Rapela, C.W. (eds.). *The Proto-Andean Margin of Gondwana*. London, Geological Society, 142 (Special Publications), 181–217.
- Rapela, C.W., Baldo, E.G., Pankhurst, R.J., Saavedra, J., 2002. Cordierite and leucogranite formation during emplacement of highly peraluminous magma: the El Pilón granite complex (Sierras Pampeanas, Argentina). *Journal of Petrology*, 43(6), 1003–1028.
- Rapela, C.W., Pankhurst, R.J., Casquet, C., Fanning, C.M., Baldo, E.G., González-Casado, J.M., Galindo, C., Dahlquist, J., 2007. The Río de la Plata craton and the assembly of SW Gondwana. *Earth Science Review*, 83(1–2), 49–82.
- Sato, K., Tassinari, C.C.G., Basei, M.A.S., Siga, O.Jr., Onoe, A.T., Dias de Souza, M., 2014. Sensitive High Resolution Ion Microprobe (SHRIMP IIe/MC) of the Institute of Geosciences of the University of São Paulo, Brazil: analytical method and first results. *Geologia USP Série Científica São Paulo*, 14(3), 3–18.
- Schaltegger, U., Fanning, C.M., Günther, D., Maurin, J.C., Schulmann, K., Gebauer, D., 1999. Growth, annealing and recrystallization of zircon and preservation of monazite in high-grade metamorphism: conventional and in-situ U-Pb isotope, cathodoluminescence and microchemical evidence. *Contributions to Mineralogy and Petrology*, 134, 186–201.
- Schärer, U., 1984. The effect of initial ^{230}Th disequilibrium on young U-Pb ages: The Makalu case, Himalaya. *Earth and Planetary Science Letters*, 67, 191–204.
- Schwartz, J.J., Gromet, L.P., 2004. Provenance of Late Proterozoic–early Cambrian basin, Sierras de Córdoba, Argentina. *Precambrian Research*, 129, 1–21.
- Schwartz, J.J., Gromet, L.P., Miró, R., 2008. Timing and Duration of the Calc-Alkaline Arc of the Pampean Orogeny: Implications for the Late Neoproterozoic to Cambrian Evolution of Western Gondwana. *The Journal of Geology*, 116, 39–61.
- Siegesmund, S., Steenken, A., Martino, R., Wemmer, K., López de Luchi, M.G., Frei, R., Presnyakow, S., Guerschi, A., 2010. Time constraints on the tectonic Evolution of the Eastern Sierras

- Pampeanas (Central Argentina). International Journal Earth Sciences, 99, 1199-1226.
- Sims, J., Ireland, T.R., Camacho, A., Lyons, P., Pieters, P.E., Skirrow, R., Stuart-Smith, PG., Miró, R., 1998. U-Pb, Th-Pb, and Ar-Ar geochronology from the Southern Sierras Pampeanas, Argentina: implications for the Paleozoic tectonic evolution of the western Gondwana margin. In: Pankhurst, R.J., Rapela, C.W. (eds.). *The Proto-Andean Margin of Gondwana*. London, Geological Society, 142 (Special Publications), 259-281.
- Sláma, J., Kosler, J., Condon, J.K., Crowley, J.L., Gerdes, A., Hanchar, J.M., Horstwood, M.S.A., Morris, G.A., Nasdala, L., Norberg, N., Schaltegger, U., Schoene, B., Tübbert, M.N., Whitehouse, M.J., 2008. Plešovice zircon-A new natural reference material for U-Pb and Hf isotopic microanalysis. *Chemical Geology*, 249, 1-35.
- Stuart-Smith, PG., Camacho, A., Sims, J.P., Skirrow, R.G., Lyons, P., Pieters, P.E., Black, L.P., 1999. Uranium – lead dating of felsic magmatic cycles in the southern Sierras Pampeanas, Argentina: Implications for the tectonic development of the proto-Andean Gondwana margin. In: Ramos, V.A., Keppie, J.D. (eds.). *Laurentia-Gondwana Connections before Pangea*. Geological Society of America, 336 (Special Papers), 87-114.
- Sun, S.S., McDonough, W.F., 1989. Chemical and isotopic systematics of oceanic basalts: implications for mantle composition and processes. In: Sun, S.S., McDonough, W.F. (eds.). *Magmatism in the Ocean Basins*. London, Geological Society, 42 (Special Publications), 313-45.
- Tibaldi, A.M., Otamendi, J.E., Gromet, L.P., Demichelis, A. H., 2008. Suya Taco and Sol de Mayo mafic complexes from eastern Sierras Pampeanas, Argentina: Evidence for the emplacement of primitive OIB-like magmas into deep crustal levels at a late stage of the Pampean orogeny. *Journal of South American Earth Sciences*, 26, 172-187.
- Toselli, A.J., 1990. Metamorfismo del Ciclo Pampeano. In: Acenolaza, F.G., Miller, H., Toselli, A.J. (eds.). *El Ciclo Pampeano en el Noroeste Argentino*. Universidad Nacional de Tucumán, Serie Correlación Geológica, 4, 181-198.
- Turner, J.C.M., 1960. Estratigrafía de la Sierra de Santa Victoria y adyacencias. *Boletín de la Academia Nacional de Ciencias*, 41, 163-196.
- Vanderhaeghe, O., Teyssier, C., Wysoczanski, R., 1999. Structural and geochronological constraints on the role of partial melting during the formation of the Shuswap metamorphic core complex at the latitude of the Thor-Odin dome, British Columbia. *Canadian Journal of Earth Sciences*, 36, 917-943.
- Vavra, X., Schmid, R., Gebauer, D., 1999. Internal morphology, habitat and U-Th-Pb microanalysis of amphibolite-to-granulite facies zircons: Geochronology of the Ivrea Zone (Southern Alps). *Contributions to Mineralogy and Petrology*, 134, 380-404.
- Von Gosen, W., Prozzi, C., 2010. Pampean deformation in the Sierra Norte de Córdoba, Argentina: implications for the collisional history at the western pre-Andean Gondwana margin. *Tectonics*, 29, 1-33.
- Weinberg, R.F., Mark, G., 2008. Magma migration, folding, and disaggregation of migmatites in the Karakoram Shear Zone, Ladakh, NW India. *Geological Society of America Bulletin*, 120(7/8), 994-1009.
- Weinberg, R.F., Becchio, R., Fariñas, P., Susaño, N., Sola, A., 2018. Early Paleozoic accretionary orogenies in NW Argentina: Growth of West Gondwana. *Earth-Science Reviews*, 187, 219-247.
- Whitney, D.L., Teyssier, C., Fayon, A.K., Hamilton, M.A., Heizler, M., 2003. Tectonic controls on metamorphism, partial melting, and intrusion: timing and duration of regional metamorphism and magmatism in the Niğde Massif, Turkey. *Tectonophysics*, 376(1-2), 37-60.
- Zeck, H.P., Whitehouse, M.J., 1999. Hercynian, Pan-African, Proterozoic and Archean ion-microprobe zircon ages for a Betic-Rif core complex, Alpine belt, W Mediterranean-consequences for its P-T-t path. *Contributions to Mineralogy and Petrology*, 134, 134-149.

Manuscript received December 2019;
revision accepted August 2020;
published Online November 2020.